Microfluidic time-division multiplexing accessing (TDMA) resistive pulse sensor for particle analysis

Gihoon Choi [a†], Erica Murphy [a†], and Weihua Guan [a, b*]

[a] Department of Electrical Engineering, Pennsylvania State University, University Park, PA, 16802, USA

[b] Department of Biomedical Engineering, Pennsylvania State University, University Park, PA, 16802, USA

† These authors contributed equally to this work.

* Correspondence should be addressed to W. Guan, Email: w.guan@psu.edu

ABSTRACT

Due to its simplicity and robustness, pore-based resistive pulse sensors have been widely used to detect, measure, and analyze particles at length scales ranging from nanometers to micrometers. While multiple pore-based resistive pulse sensors are preferred to increase the analysis throughput and to overcome the clogging issues, the scalability is often limited. In response, by combining the time-division multiple access technique in the telecommunication field with the microfluidics, we reported a microfluidic time-division multiplexing accessing (TDMA) single-end resistive pulse sensor, in which particles can be analyzed through a scalable number of microfluidic channels. With an eight-channel microfluidic device and polystyrene particles as proof-of-principle, we successfully demonstrated this multiplexed technology is effective in measuring the particle size and concentration, in analyzing the particle arriving dynamics, and in discriminating mixed populations. Importantly, the availability of multiple sensing pores provides a robust mechanism to overcome the clogging issue, allowing the analysis to continue even when some of the pores are clogged. We anticipate this TDMA approach could find wide applications and facilitate future development of multiplexed resistive pulse sensing from microscale to nanoscale.

KEYWORDS

Resistive pulse sensor, micropore, nanopore, time-division multiple access, multiplexed

Coulter counters, also known as the resistive pulse sensors, are well-developed devices to measure the size and concentration of biological cells and colloidal particles suspended in a buffer solution[1]. In Coulter devices, including its microfluidic versions, two electrolyte-filled compartments or chambers are separated by a microscopic conduction path. When a particle flows through this orifice, the devices' electrical resistance is temporarily changed. This resistance change is often measured as a current dip, the magnitude and the duration of which is correlated to size, shape, mobility, surface charge, and concentration of the particles[2-8]. Due to its simplicity and robustness, the resistive pulse sensor has been used for a variety of applications[9-18], ranging from the analysis of blood cells[10, 14, 19-20], bacteria[21-22] and viruses[18, 23] to the detection and counting of colloidal particles[24-25] and pollen[9]. Besides, nanoscale Coulter counter devices such as nanopores[26-30] were also developed to detect biomolecules such as proteins[26-27] and DNAs[28].

Whether working in the microscale or the nanoscale, most resistive pulse sensor experiments would require measuring sufficient numbers of single particle translocations to generate meaningful statistics for analysis. In this regard, multichannel systems have a clear advantage in terms of faster data collection and analysis throughput. Integration of multiple channels into the same device also enables the analysis of the same sample with different experimental parameters such as applied voltage and pore size. Besides, multiple pores also help to keep the analysis running even one or few of the pores are clogged, a grand challenge in resistive pulse sensors[31-32]. In recognition of these benefits, efforts to simultaneously record multiple channels were pursued in micropores[33] and nanopores[34-36], often with multi-channel patch clamp amplifier. However, the scalability of the channel numbers is limited by the cost because each fluidic channel would require an independent measuring unit. An ideal multiplexed resistive pulse sensor should have a single output to easily interface with the single-input instrument. To this end, one method employs the

frequency division multiplexing for multichannel, single-output resistive pulse sensing. Signals from multiple channels are modulated by an AC signal with a single frequency and then recovered by digital bandpass filtering[37]. Another method emulates the radio communication technique of code-division multiple access (CDMA) to achieve an all-electronic, single-output interface[38]. As particles traverse encoding electrodes, orthogonal digital codes are generated. Software algorithms were used to decode the output signal to correlate each resistive pulse with its channel of origin.

Herein, we reported a microfluidic time-division multiplexing accessing (TDMA) single-end resistive pulse sensor for particle analysis. In the cellular communication field, TDMA allows multiple users to communicate with a base station over a common channel through time-sharing[39]. The microfluidic TDMA resistive pulse sensor adopts a similar principle to multiplex the signal from many different fluidic channels. With a single-ended data acquisition, signals from each channel can be reconstructed for particle analysis in the corresponding channels. We successfully demonstrated a low-cost eight-channel microfluidic resistive pulse sensor for analyzing the size and concentration of polystyrene particles. Further scaling up the multiplexity is straightforward and within reach. We also found that the multiplexed TDMA device is able to continue the analysis even when a few channels are clogged, solving one of the most significant challenges in resistive pulse sensors. We anticipate this single-ended time-shared approach is widely applicable and would facilitate the development of multiplexed resistive pulse sensing from microscale to nanoscale.

EXPERIMENTAL SECTION

Materials and chemicals

10- and 15-μm diameter polystyrene particles (coefficient variance <10%) were purchased from Polyscience. Prior to the experiment, the sample concentrations were diluted using phosphate buffered saline (PBS) (1X, pH 7.4) with 0.05% Tween 20 (TEKnova) to avoid particle aggregation. Ag/AgCl electrodes were manufactured by chloriding silver wires (ϕ = 0.375 mm, Warner Instruments) in 1M KCl solution (Sigma-Aldrich). A small hole was punched from the outside wall of the tygon tubing and Ag/AgCl electrodes were threaded through this hole into the inside of the tube, followed by epoxy sealing. This customized tubing provides both electrical and fluidic access to the microfluidic device.

Microfluidic device fabrication

An eight-channel microfluidic device was designed using CAD software (**Supplementary Figure S1**). The photomask was printed on transparent film (CAD/Art Services, Inc.). The casting mold was fabricated on a 4-inch silicon wafer using SU-8 2025 (MicroChem) through a standard lithography process. The mold height of ~35 μm was confirmed with a profilometer. The width and length of the micropore were optimized to ~18 μm and ~20 μm respectively. The microfluidic device was fabricated using the polydimethylsiloxane (PDMS) (Dow Corning). A 10:1 w/w mixture of base and curing agent was cast onto the SU-8 wafer mold, degassed, and cured at 80°C for an hour. After demolding the patterned PDMS, inlet and outlets were punched using a stainless needle (ϕ = 0.75 mm). The resulting PDMS stamps and glass slides (100 μm thickness, ted-Pella) were treated with oxygen plasma and in contact to form irreversibly covalent bonding between two materials.

TDMA hardware instrumentation

The TDMA hardware circuit was implemented on a custom printed circuit board (PCB) (OSH

Park), which includes trans-impedance amplifiers (TL072, Texas Instruments), analog multiplexer (ADG406, Analog Devices), and counter (dual negative-edge-triggered JK flip-flop: 74LS73, Texas Instruments; 2-input AND gate: DM7408, Fairchild Semiconductor^{TM}) (**Supplementary Figure S2**). Eight sensing units from the microfluidic device were connected to trans-impedance amplifiers. A feedback resistor (R= 1 MΩ with 5% tolerance) was used to set the gain. The amplifier outputs were connected as inputs to the multiplexer. The multiplexer channels were periodically selected by a $\log_2(N)$ bit synchronous counter. The sampling frequency for each TDMA frame was synchronized to the multiplexer switching frequency. The analog voltage output from multiplexer was sampled at 200 kHz with 16-bit DAQ card (NI PCIe-6351, National Instruments) and stored through a data acquisition software (LabVIEW, National Instruments). The recorded data were demultiplexed using MATLAB (MathWorks) program.

Electrical measurement

The microfluidic channels were prefilled with electrolyte (1x PBS with 0.05% Tween-20) for electrical measurement. The customized tygon tubes with Ag/AgCl electrodes embedded were inserted into the punched holes on the microfluidic devices. The outlets were grounded while the inlet was biased at a constant voltage (400 mV). The ionic currents from each sensing unit were monitored by custom-built eight channel TDMA hardware, which performed current-to-voltage conversion and analog signal multiplexing. The ionic current level decreased during the particle translocation due to the increase of resistance at the micropore area. The electrical measurement was performed inside a customized Faraday cage to shield the environment noise. The sample was introduced at a constant flow rate using a syringe pump (Harvard Apparatus PHD 2000).

Particle size and concentration calculation

Resistive pulse sensing has been extensively studied for the nano- and micron-ranged particle size analysis [1, 33, 40-45]. The relative resistance changes ($\Delta R/R$) caused by particle translocation at a sensing pore is described by the following particle sizing equation[46],

$$\frac{\Delta R}{R} = \frac{D}{L}\left[\frac{\arcsin(d/D)}{\sqrt{1-(d/D)^2}} - \frac{d}{D}\right] \quad (1)$$

where d is particle diameter, D and L are cylindrical orifice diameter and length, respectively. For the rectangular micropore, we substitute $D = (4\times W\times H/\pi)^{1/2}$, where W and H are a sensing pore width and a height, respectively. $\Delta R/R$ was extracted from the data using MATLAB (MathWorks), and particle diameters were obtained by Eq. 1. Note this particle sizing model does not take into consideration the correction factor[46] and thus can lead to uncertainty in size determination.

To calculate the particle concentration, total particle counts from the eight sensing units were divided by the total introduced sample volume. The total particle counts were extracted by counting the resistive pulses using the peak-detection algorithm in MATLAB (**Supplementary Figure S3**). The total introduced sample volume was obtained from multiplying volume flow rate by the elapsed time.

RESULTS AND DISCUSSION

Working principles

Figure 1a shows the block diagram of the microfluidic TDMA system designed to interface the N-channel microfluidic resistive pulse sensor. The integrated TDMA system consists of the transimpedance amplifiers, an analog multiplexer, analog-to-digital converter (A/D), and demultiplexer. The multiplexer sequentially reads the amplified analog signals from each sensing

channel with a switching frequency of f_s , in other words, each channel is sampled every N/f_s second (*i.e.,* the period of a single TDMA frame, the top panel in **Figure 1b**) and digitalized by an A/D for data acquisition. A demultiplexing algorithm reconstructs the signal for each channel using the scheme shown in **Figure 1b**. It is noteworthy that there is a tradeoff between the channel multiplexity N and the effective channel sampling frequency using a fixed switching frequency.

In our proof-of-principle study, we implemented an eight-channel microfluidic device with a circular layout (**Supplementary Figure S1).** All eight channels have separated outlets, yet share a common inlet (**Figure 1c**). A micro-filter structure is designed near the common inlet to remove the potential debris. In a typical experiment, the polystyrene particle translocation time was in the range of 8±2.7 ms (**Supplementary Figure S4**). To resolve the single particle translocation event, each channel should have a minimum sampling frequency higher than the Nyquist frequency (250 Hz). We used a switching frequency f_s of 200 kHz for the eight-channel implementation. The equivalent single-channel sampling frequency is 25 kHz, sufficient for resolving the single particle translocation. In fact, the channel multiplexity can be scaled up to 800 if we work at the minimal Nyquist frequency. Note that this TDMA principle could also be extended to nanopore sensors[34-36], in which single-molecule translocation is usually much faster. For a typical dwell time as short as 100 μs[47], the same 200 kHz switching frequency is sufficient to resolve ten channels.

Validation of the TDMA principle

To validate the 8-channel microfluidic resistive pulse sensor and the TDMA scheme, we tested polystyrene particles of 10 μm diameter at a concentration of ~2.4×10^5 particles/ml. Before sample loading, all microfluidic channels were filled with 1x PBS buffer with 0.05% Tween-20 to remove potential air bubbles. The prepared sample was introduced into the inlet of the microfluidic device with a flow rate of 200 μl/hr. The signal from each of the eight channels was sequentially switched

at 200 kHz into one single output by the TDMA hardware. The digitalized combined signal was then demultiplexed to reconstruct the time trace signal for each channel. **Figure 2a** shows the demultiplexed current time traces for all eight channels. Apparent ionic current dips, corresponding to individual particle translocation events, could be easily observed from all channels. These current dips were uniform in magnitude due to the introduced monodisperse particles.

One of the concerns in TDMA resistive pulse sensing is the interference due to the signal leakage in analog switching networks. The current dips in **Figure 2a** appear in random sequence, implying that each channel can independently analyze the particles without crosstalk among channels. To quantify the channel-to-channel crosstalk, we performed the cross-correlation analysis of ionic current profiles among eight sensing channels and extracted the Pearson correlation coefficient. **Figure 2b** shows the heatmap of the correlation between channels. The inter-channel correlation is quite small (with coefficient ranging from -0.25 to 0.32), confirming the signal integrity in each channel. Interestingly, the correlation seems alternating between the positive and negative value for channels separated by odd and even numbers, which is likely due to the characteristics of the switching networks.

Probing the particle arriving dynamics

A quick eyeball on the current time traces in **Figure 2a** reveals that the particle translocation frequency varies among different channels. To probe the particle arriving dynamics, we examined the event inter-arrival time distribution for each channel. As shown in **Figure 3a,** the inter-arrival time distribution shows a remarkable exponential distribution for each channel, indicating a Poisson process[48]. Each channel was fitted with an exponential distribution, $P(t) = \lambda e^{-\lambda t}$, where λ is the expected particle translocation rate. As shown in **Figure 3a,** the particle arriving rates

among different channels ranges from 0.79 s^{-1} to 3.12 s^{-1}, implying the introduced particles prefer certain channels. This is likely because the effective dimension for each sensing pore is not perfectly identical due to variations in the fabrication and the potential adsorption during the experiment. This creates asymmetric streamlines that lead the particles into preferred channels.

To further examine whether the observed Poisson process is homogenous or nonhomogeneous, we plotted the accumulative particle number versus the elapsed time. As shown in **Figure 3b,** the slope of the curve (*i.e.,* the translocation rate) is different among channels, consistent with what we observed from **Figure 3a.** However, the slope of the curve for each channel shows a clear time-dependence. This indicates the translocation rate for sub-processes indeed varies. Therefore, the particle translocation process of our experiment is a nonhomogeneous Poisson process.

Analyzing particle size and concentration

To test the multiplexed TDMA resistive pulse sensor for particle sizing, we extracted the relative resistance changes ($\Delta R/R$) from the detected resistive peaks in **Figure 2a**. To determine the particle size, we applied the particle sizing model using Eq. 1. **Figure 4a** shows the particle diameter distribution in each channel, together with a combined distribution from all channels. The combined distribution follows a Gaussian distribution with a mean value of ~9.5±0.54 μm. The calculated particle diameter is comparable, yet smaller than the actual particle size (10 μm). The under-estimation of the particle diameter may come from the fact that the particle sizing model assumes particles pass through the centerline of the pore[45]. Motion displacement from the center axis could cause the underestimation. It was also observed that the mean particle diameter varies among eight individual channels (**Figure 4a**). This is likely due to the channel-to-channel size variation during the device fabrication and during the experiments (*e.g.*, adsorption of small debris near the pore region). Strategies to improve each of these issues could help to narrow the size

distribution.

Since each current dip event represents a single particle and the particle arriving events follow the Poisson process (**Figure 3**), the particle concentration at 95% confidence interval was calculated as $(n \pm 1.96(n)^{1/2})/(vT)$, where n is the total number of particles counted from all 8 channels, T is the total elapsed time, and v is the volume flow rate. The relative uncertainty of inferring the concentration is proportional to $n^{-1/2}$. **Figure 4b** shows the calculated concentration as a function of total counted particles. After counting about 1000 particles, the calculated concentration converges to that of the input sample (2.4×10^5 particles/ml) with little uncertainty.

Analyzing a mixed population

To test the microfluidic multiplexed TDMA resistive pulse sensor for analyzing a mixed population, we prepared a mixed sample containing 10 μm and 15 μm polystyrene particles with concentrations of ~2.4×10^5 ml^{-1} and ~0.8×10^5 ml^{-1}, respectively. **Figure 5a** shows the demultiplexed current time traces for all eight channels, and **Figure 5b** shows an enlarged section from channel 4 (red boxed area). As expected, we observed two distinct levels of current dips, corresponding to the two size populations. Other channels also show similar two population characteristics. Using the particle sizing model (Eq. 1) and combing events from all channels, the particle sizes were calculated, and their distribution is shown in **Figure 5c.** The particle size distribution shows evident two populations with a mean value of 9.31 ± 0.40 μm (10 μm particle population) and 12.46 ± 0.48 μm (15 μm particle population), respectively. The underestimation for each population is likely due to the same reason as we saw in **Figure 4a.** The particle numbers counted for each population is 1233 and 355, the ratio of which (~3.47) is close to that of the input concentration value (~3), confirming the discriminative ability between these two populations.

Robustness against pore clogging

While we did not see any clogging issue when testing the 10 μm sized particles (**Figure 2a**), a clear feature observed in **Figure 5a** when testing the 15 μm sized particles is that two out of eight channels (channel 6 and 7) show no particle translocation events. We examined the sensing pores using a microscope after the experiment. It was found that channel 6 and 7 were indeed clogged by particle jamming at the pore (**Figure 5d**). This is not surprising since the pore cross-section is of dimension 18 μm×20 μm×35 μm (W×L×H). When 15 μm sized particles were introduced, the chance for clogging becomes much higher. Such irreversible clogging is a well-known issue for single-channel resistive pulse sensors that limits its flexibility in real-world applications[31-32]. In contrast, the TDMA multichannel resistive pulse sensor allows the analysis to continue even when some of the pores are clogged (**Figure 5c**). We anticipate that future works could introduce an array of different pore sizes for analyzing polydisperse samples.

CONCLUSION

By introducing the time-division multiple access technique in the telecommunication field into the microfluidic field, we developed and demonstrated the multiplexed microfluidic resistive pulse sensor, in which particles can be analyzed simultaneously by a scalable number of microfluidic channels. The microfluidic TDMA resistive pulse sensing technology allows each channel to transmit its temporal signal in rapid succession to a single electrical outlet, using a defined time slot with a defined order, which can then be used to recover the signal from each channel by a simple demultiplexing algorithm. With the prototyped TDMA instrumentation and the eight-channel microfluidic device, we demonstrated this multiplexed microfluidic TDMA technology is readily useful in measuring the particle size and concentration, in analyzing the particle arriving

dynamics, and in discriminating mixed populations. In particular, the availability of multiple sensing pores provides a robust mechanism to fight against the clogging issue, allowing the analysis to continue, which is otherwise not possible in single channel devices. While the TDMA resistive pulse sensing technology is validated in microfluidic devices in this study, we expect this proof-of-concept could be well extended to nanoscale resistive pulse sensors such as nanopores [49].

ACKNOWLEDGMENTS

This work supported by the National Science Foundation under Grant No. 1710831. Any opinions, findings, and conclusions or recommendations expressed in this work are those of the authors and do not necessarily reflect the views of the National Science Foundation. W.G. acknowledges the support from Penn State Startup Fund.

ASSOCIATED CONTENT

The Supporting Information is available.

Particle sizing model, microfluidic device layout, TDMA hardware (electronic circuit diagram and PCB layout), validation of a peak-detection algorithm for resistive pulse sensing and a typical polystyrene particle translocation time and ionic current dip information.

AUTHOR INFORMATION

Corresponding Authors

* Email: w.guan@psu.edu

ORCID

Weihua Guan: 0000-0002-8435-9672

Author contributions

W.G. conceived and supervised the study. G.C. fabricated the microfluidic device. E.M. implemented TDMA hardware and software. G.C. and E.M. performed the sensing experiments. All authors analyzed the results and wrote the manuscript.

NOTES

The authors declare no competing financial interest.

FIGURES AND CAPTIONS

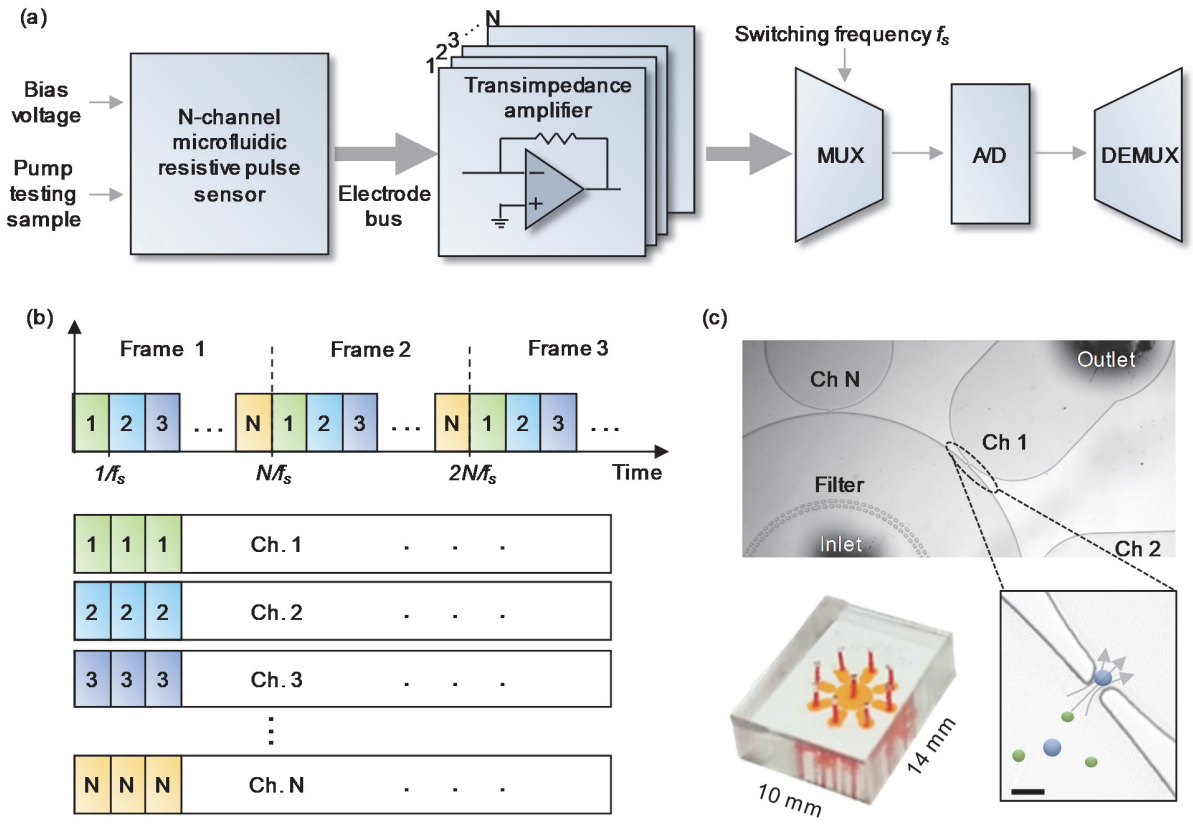

Figure 1. TDMA resistive pulse sensor working principles. (a) Time-division multiple access block diagrams. (b) Illustration of the demultiplexing algorithm. The serial signal from multiplexer output was reconstructed for each channel. (c) Microscope images of the 8-plexed device. The enlarged image illustrates the particle translocation through the sensing pore. A micro-filter is placed upstream to reduce the potential debris.

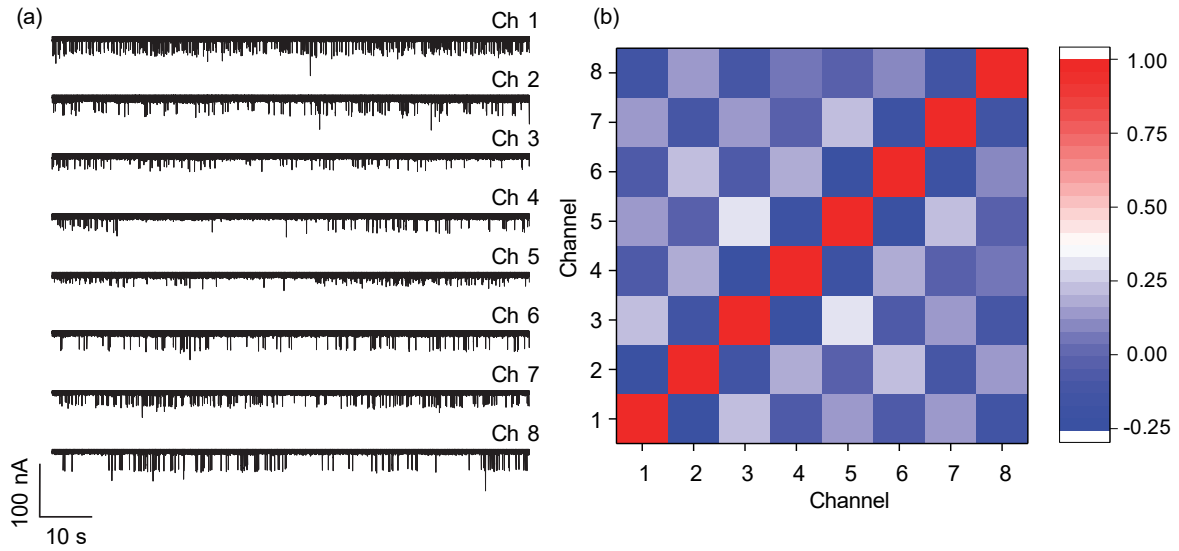

Figure 2. Validation of TDMA resistive pulse sensor. (a) Reconstructed current time trace for each of the eight channels. (b) Cross-correlation among different sensing channels.

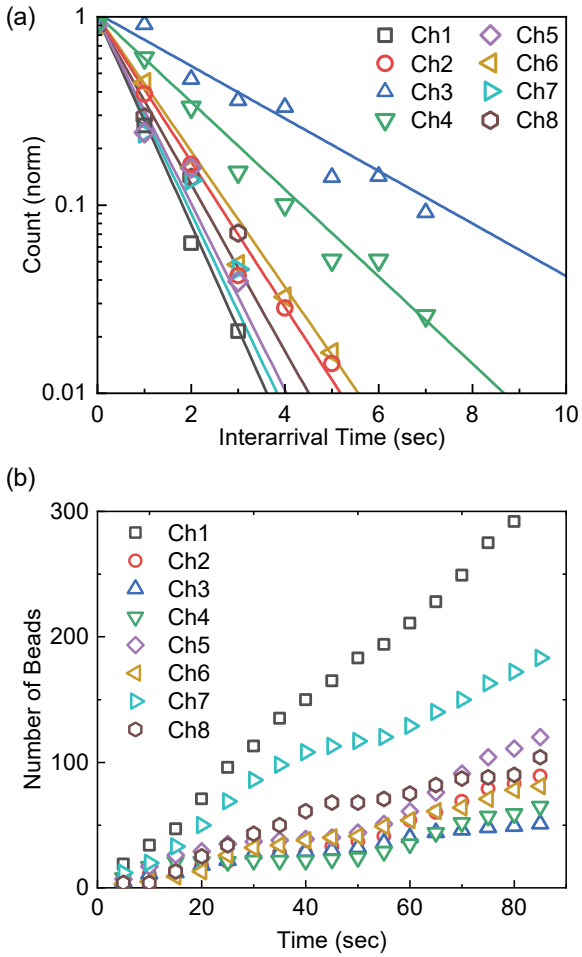

Figure 3. Particle translocation dynamics. (a) The normalized distribution of bead interarrival time in different channels, with exponential fits to the distributions (λ_{ch1}: 3.12 s^{-1}, λ_{ch2}: 0.98 s^{-1}, λ_{ch3}: 0.79 s^{-1}, λ_{ch4}: 0.83 s^{-1}, λ_{ch5} 1.21 s^{-1}, λ_{ch6}: 0.88 s^{-1}, λ_{ch7}: 1.88 s^{-1}, and λ_{ch8}: 1.13 s^{-1}). (b) Cumulative counted particle numbers versus the elapsed time.

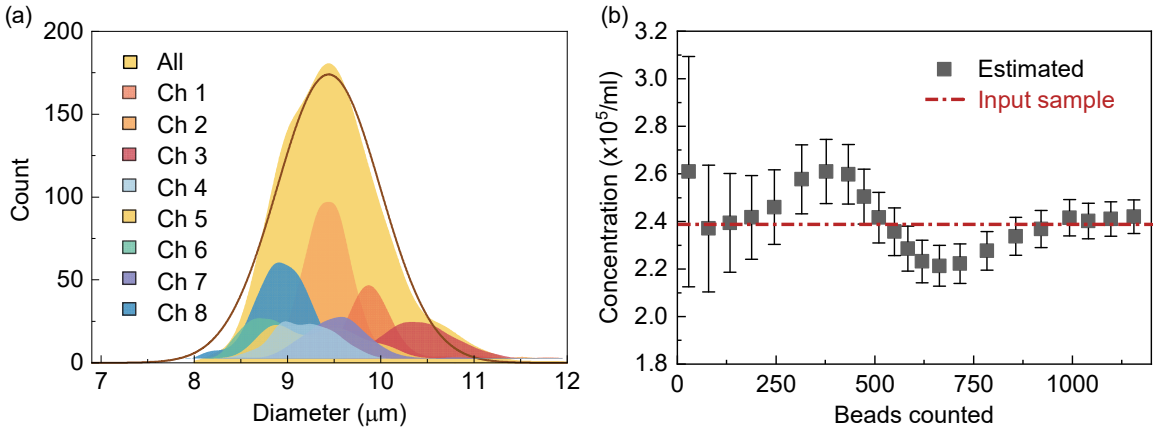

Figure 4. Particle size and concentration measurement. (a) Histograms of the calculated particle diameters from each individual sensing channel (N_{Ch1}:131, N_{Ch2}: 309, N_{Ch3}:104, N_{Ch4}: 97, N_{Ch5}:124, N_{Ch6}: 94, N_{Ch7}:102, N_{Ch8}: 223). Distribution of the entire particle diameter data set was plotted with Gaussian-fit (N_{All}: 1184). (b) Calculated concentration as a function of the counted particles. The error bars correspond to the Poisson noise. The actual polystyrene particle concentration (~2.4×10^5 particles/ml) is indicated by the red dashed line.

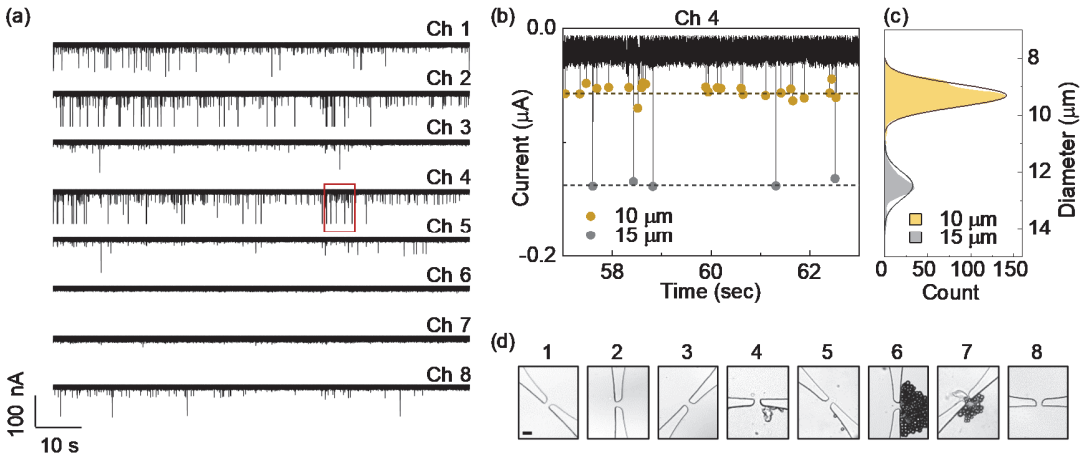

Figure 5. Discriminating particles of different size. (a) Reconstructed current time trace for each of the eight channels. (b) Enlarged view of ionic current in channel 4 (red) showing representative pulses from a mixture of 10 µm and 15 µm diameter particles. (c) Distribution of the particle size, with Gaussian-fit. A clear two population was observed. ($N_{10\mu m}$: 1233 and $N_{15\mu m}$: 355). (d) Microscope images showing the pore clogging in channel 6 and 7. (Scale bar: 20 µm).

Reference

1. Song, Y.; Zhang, J.; Li, D., Microfluidic and Nanofluidic Resistive Pulse Sensing: A Review. *Micromachines* **2017,** *8* (7), 204. DOI: 10.3390/mi8070204
2. Gawad, S.; Schild, L.; Renaud, P. H., Micromachined impedance spectroscopy flow cytometer for cell analysis and particle sizing. *Lab Chip* **2001,** *1* (1), 76-82.
3. Watkins, N.; Venkatesan, B. M.; Toner, M.; Rodriguez, W.; Bashir, R., A robust electrical microcytometer with 3-dimensional hydrofocusing. *Lab Chip* **2009,** *9* (22), 3177-3184.
4. Nasir, M.; Ateya, D. A.; Burk, D.; Golden, J. P.; Ligler, F. S., Hydrodynamic focusing of conducting fluids for conductivity-based biosensors. *Biosensors & bioelectronics* **2010,** *25* (6), 1363-1369.
5. Dhawan, A. P.; Heetderks, W. J.; Pavel, M.; Acharya, S.; Akay, M.; Mairal, A.; Wheeler, B.; Dacso, C. C.; Sunder, T.; Lovell, N.; Gerber, M.; Shah, M.; Senthilvel, S. G.; Wang, M. D.; Bhargava, B., Current and Future Challenges in Point-of-Care Technologies: A Paradigm-Shift in Affordable Global Healthcare With Personalized and Preventive Medicine. *IEEE J. Transl, Eng. He.* **2015,** *3*, 1-10.
6. Emaminejad, S.; Paik, K. H.; Tabard-Cossa, V.; Javanmard, M., Portable cytometry using microscale electronic sensing. *Sens. Actuators, B* **2016,** *224*, 275-281.
7. Spencer, D.; Caselli, F.; Bisegna, P.; Morgan, H., High accuracy particle analysis using sheathless microfluidic impedance cytometry. *Lab Chip* **2016,** *16* (13), 2467-2473.
8. Garboczi, E. J., The influence of particle shape on the results of the electrical sensing zone method as explained by the particle intrinsic conductivity. *Powder Technol* **2017,** *322*, 32-40.
9. Zheng Zhang, J. Z., Santanu Chandra, Jun Hu, An electronic pollen detection method using Coulter counting principle. *Atmospheric Environment* **2005,** *39* (30), 5446-5453.
10. Holmes, D.; Pettigrew, D.; Reccius, C. H.; Gwyer, J. D.; van Berkel, C.; Holloway, J.; Davies, D. E.; Morgan, H., Leukocyte analysis and differentiation using high speed microfluidic single cell impedance cytometry. *Lab Chip* **2009,** *9* (20), 2881-2889.
11. Hua, S. Z.; Pennell, T., A microfluidic chip for real-time studies of the volume of single cells. *Lab Chip* **2009,** *9* (2), 251-256.
12. Bernabini, C.; Holmes, D.; Morgan, H., Micro-impedance cytometry for detection and analysis of micron-sized particles and bacteria. *Lab Chip* **2011,** *11* (3), 407-412.
13. van Berkel, C.; Gwyer, J. D.; Deane, S.; Green, N. G.; Holloway, J.; Hollis, V.; Morgan, H., Integrated systems for rapid point of care (PoC) blood cell analysis. *Lab Chip* **2011,** *11* (7), 1249-1255.
14. Evander, M.; Ricco, A. J.; Morser, J.; Kovacs, G. T. A.; Leung, L. L. K.; Giovangrandi, L., Microfluidic impedance cytometer for platelet analysis. *Lab Chip* **2013,** *13* (4), 722-729.
15. Zheng, Y.; Nguyen, J.; Wei, Y.; Sun, Y., Recent advances in microfluidic techniques for single-cell biophysical characterization. *Lab Chip* **2013,** *13* (13), 2464-2483.
16. Rodriguez-Trujillo, R.; Ajine, M. A.; Orzan, A.; Mar, M. D.; Larsen, F.; Clausen, C. H.; Svendsen, W. E., Label-free protein detection using a microfluidic Coulter-counter device. *Sens. Actuators, B* **2014,** *190*, 922-927.
17. Murphy, T. W.; Zhang, Q.; Naler, L. B.; Ma, S.; Lu, C., Recent advances in the use of microfluidic technologies for single cell analysis. *The Analyst* **2018,** *143* (1), 60-80.
18. Watkins, N. N.; Hassan, U.; Damhorst, G.; Ni, H. K.; Vaid, A.; Rodriguez, W.; Bashir, R., Microfluidic CD4(+) and CD8(+) T Lymphocyte Counters for Point-of-Care HIV Diagnostics Using Whole Blood. *Sci Transl Med* **2013,** *5* (214), 214ra170(1-11).

19. van Berkel, C.; Gwyer, J. D.; Deane, S.; Green, N. G.; Holloway, J.; Hollis, V.; Morgan, H., Integrated systems for rapid point of care (PoC) blood cell analysis. *Lab Chip* **2011,** *11* (7), 1249-1255.
20. Yang, X. N.; Chen, Z. F.; Miao, J.; Cui, L. W.; Guan, W. H., High-throughput and label-free parasitemia quantification and stage differentiation for malaria-infected red blood cells. *Biosensors & bioelectronics* **2017,** *98*, 408-414.
21. Yu, A. C. S.; Loo, J. F. C.; Yu, S.; Kong, S. K.; Chan, T. F., Monitoring bacterial growth using tunable resistive pulse sensing with a pore-based technique. *Appl. Microbiol. Biotechnol.* **2014,** *98* (2), 855-862.
22. Song, Y. X.; Zhang, H. P.; Chon, C. H.; Chen, S.; Pan, X. X.; Li, D. Q., Counting bacteria on a microfluidic chip. *Anal. Chim. Acta* **2010,** *681* (1-2), 82-86.
23. Yang, L.; Yamamoto, T., Quantification of Virus Particles Using Nanopore-Based Resistive-Pulse Sensing Techniques. *Frontiers in microbiology* **2016,** *7*, 1500. DOI: 10.3389/fmicb.2016.01500
24. Saleh, O. A.; Sohn, L. L., Quantitative sensing of nanoscale colloids using a microchip Coulter counter. *Rev. Sci. Instrum.* **2001,** *72* (12), 4449-4451.
25. Zhang, W. C.; Hu, Y.; Choi, G.; Liang, S. F.; Liu, M.; Guan, W. H., Microfluidic multiple cross-correlated Coulter counter for improved particle size analysis. *Sensors and Actuators B: Chemical* **2019,** *296* (126615). DOI: 10.1016/j.snb.2019.05.092
26. Waduge, P. a. H., R. and Bandrakar, P and Yamazaki, H and Cressiot, B and Zhao, Q. and Whitford, P and Wanunu, M, Nanopore-Based Measurements of Protein Size, Fluctuations, and Conformational Changes. *Acs Nano* **2017,** *11* (5), 5706-5716.
27. Hoogerheide, D. P.; Gurnev, P. A.; Rostovtseva, T. K.; Bezrukov, S. M., Real-Time Nanopore-Based Recognition of Protein Translocation Success. *Biophysical Journal* **2018,** *114* (4), 772-776.
28. Karolis, M., E. Niklas , and U. F. Keyser, QuipuNet: Convolutional Neural Network for Single-Molecule Nanopore Sensing. *Nano letters* **2018,** *6*, 4040-4045.
29. Kidan, L.; Kyeong-Beom, P.; Hyung-Jun, K.; Jae-Seok, Y.; Hongsik, C.; Hyun-Mi, K.; Ki-Bum, K., Recent Progress in Solid-State Nanopores. *Advanced materials* **2018,** *30*, 1704680(1-28). DOI: 10.1002/adma.201704680
30. Rivas, F.; Zahid, O. K.; Reesink, H. L.; Peal, B. T.; Nixon, A. J.; DeAngelis, P. L.; Skardal, A.; Rahbar, E.; Hall, A. R., Label-free analysis of physiological hyaluronan size distribution with a solid-state nanopore sensor. *Nat. Commun.* **2018,** *9* (1), 1037. DOI: 10.1038/s41467-018-03439-x.
31. Maas, S. L. N.; de Vrij, J.; van der Vlist, E. J.; Geragousian, B.; van Bloois, L.; Mastrobattista, E.; Schiffelers, R. M.; Wauben, M. H. M.; Broekman, M. L. D.; Nolte-'t Hoen, E. N. M., Possibilities and limitations of current technologies for quantification of biological extracellular vesicles and synthetic mimics. *J. Control. Release* **2015,** *200*, 87-96.
32. Smeets, R. M. M.; Keyser, U. F.; Dekker, N. H.; Dekker, C., Noise in solid-state nanopores. *Proceedings of the National Academy of Sciences of the United States of America* **2008,** *105* (2), 417-421.
33. Zhe, J.; Jagtiani, A.; Dutta, P.; Hu, J.; Carletta, J., A micromachined high throughput Coulter counter for bioparticle detection and counting. *Journal of Micromechanics and Microengineering* **2007,** *17* (2), 304-313.
34. Osaki, T.; Suzuki, H.; Le Pioufle, B.; Takeuchi, S., Multichannel simultaneous measurements of single-molecule translocation in alpha-hemolysin nanopore array. *Anal Chem*

2009, *81* (24), 9866-70.
35. Baaken, G.; Ankri, N.; Schuler, A. K.; Ruhe, J.; Behrends, J. C., Nanopore-based single-molecule mass spectrometry on a lipid membrane microarray. *ACS Nano* **2011,** *5* (10), 8080-8.
36. Bell, N. A.; Thacker, V. V.; Hernández-Ainsa, S.; Fuentes-Perez, M. E.; Moreno-Herrero, F.; Liedl, T.; Keyser, U. F., Multiplexed ionic current sensing with glass nanopores. *Lab Chip* **2013,** *13* (10), 1859-1862.
37. Jagtiani, A. V.; Carletta, J.; Zhe, J., A microfluidic multichannel resistive pulse sensor using frequency division multiplexing for high throughput counting of micro particles. *J Micromech Microeng* **2011,** *21* (6), 065004. DOI: 10.1088/0960-1317/21/6/065004
38. Liu, R.; Wang, N.; Kamili, F.; Sarioglu, A. F., Microfluidic CODES: a scalable multiplexed electronic sensor for orthogonal detection of particles in microfluidic channels. *Lab Chip* **2016,** *16* (8), 1350-1357.
39. Ozarow, L. H.; Shamai, S.; Wyner, A. D., Information-Theoretic Considerations for Cellular Mobile Radio. *IEEE T. Veh. Technol.* **1994,** *43* (2), 359-378.
40. Smythe, W. R., Flow around a Spheroid in a Circular Tube. *Phys. Fluids* **1964,** *7* (5), 633-638.
41. Adams, R. B.; Voelker, W. H.; Gregg, E. C., Electrical Counting and Sizing of Mammalian Cells in Suspension - an Experimental Evaluation. *Phys. Med. Biol.* **1967,** *12* (1), 79-92.
42. Deblois, R. W.; Bean, C. P., Counting and Sizing of Submicron Particles by Resistive Pulse Technique. *Rev. Sci. Instrum.* **1970,** *41* (7), 909-915.
43. Saleh, O. A.; Sohn, L. L., An artificial nanopore for molecular sensing. *Nano Letters* **2003,** *3* (1), 37-38.
44. Dekker, C., Solid-state nanopores. *Nat. Nanotechnol.* **2007,** *2* (4), 209-215.
45. Gregg, E. C.; Steidley, K. D., Electrical Counting and Sizing of Mammalian Cells in Suspension. *Biophys. J.* **1965,** *5* (4), 393-405.
46. Deblois, R. W.; Bean, C. P., Counting and Sizing of Submicron Particles by the Resistive Pulse Technique. *Rev Sci Instrum* **1970,** *41* (7), 909-916.
47. Fologea, D.; Uplinger, J.; Thomas, B.; McNabb, D. S.; Li, J., Slowing DNA translocation in a solid-state nanopore. *Nano letters* **2005,** *5* (9), 1734-1737.
48. Meller, A.; Branton, D., Single molecule measurements of DNA transport through a nanopore. *Electrophoresis* **2002,** *23* (16), 2583-2591.
49. Albrecht, T., Single-Molecule Analysis with Solid-State Nanopores. *Annual Review of Analytical Chemistry* **2019,** *12*, 5.1–5.17.

For TOC only:

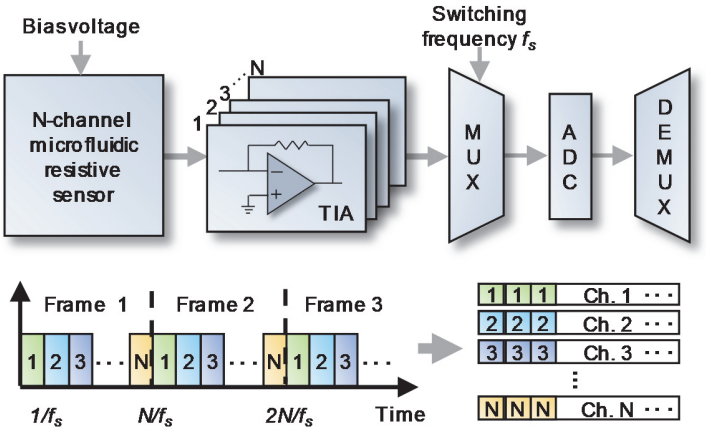
Biasvoltage
Switching frequency f_s
N-channel microfluidic resistive sensor
1
2
3
N
TIA
M U X
A D C
D E M U X
Frame 1
Frame 2
Frame 3
1 2 3 ··· N 1 2 3 ··· N 1 2 3 ···
$1/f_s$
N/f_s
$2N/f_s$
Time
1 1 1 Ch. 1 ···
2 2 2 Ch. 2 ···
3 3 3 Ch. 3 ···
N N N Ch. N ···